



On the use of NLSST and MCSST for the study of spatio-temporal trends in SST gradients

M. Bouali, P. S. Polito, O. T. Sato & J. Vazquez-Cuervo

To cite this article: M. Bouali, P. S. Polito, O. T. Sato & J. Vazquez-Cuervo (2019) On the use of NLSST and MCSST for the study of spatio-temporal trends in SST gradients, *Remote Sensing Letters*, 10:12, 1163-1171, DOI: [10.1080/2150704X.2019.1666312](https://doi.org/10.1080/2150704X.2019.1666312)

To link to this article: <https://doi.org/10.1080/2150704X.2019.1666312>



Published online: 17 Sep 2019.



Submit your article to this journal



Article views: 139



View related articles



View Crossmark data



Citing articles: 4 View citing articles



On the use of NLSST and MCSST for the study of spatio-temporal trends in SST gradients

M. Bouali^a, P. S. Polito^a, O. T. Sato^a and J. Vazquez-Cuervo^b

^aLaboratório de Oceanografia por Satélites, Instituto Oceanográfico da Universidade de São Paulo (IOUSP), São Paulo, Brazil; ^bNASA Jet Propulsion Laboratory, California Institute of Technology, Pasadena, CA, USA

ABSTRACT

Ongoing efforts are dedicated by meteorological and oceanographic agencies to improve the accuracy of Sea Surface Temperature (SST) estimates from satellite observations via improved retrieval algorithms and validation data. An important application of satellite-based SST observations is the analysis of the spatio-temporal characteristics of ocean fronts, which depend on several parameters including the SST retrieval scheme from Top-of-Atmosphere Brightness Temperatures. In this study, we focus on two widely used SST retrieval algorithms, namely the Multichannel SST (MCSST) and the Nonlinear SST (NLSST). Using night-time Level 2 SST derived from the Moderate Resolution Imaging Spectroradiometer (MODIS) onboard Aqua from 2005 to 2015 over the Southwestern Atlantic Ocean (SAO), we show that 1) the spatial distribution and temporal variability of SST gradient magnitudes derived from these two SST retrieval schemes are different despite statistical consistency of SST fields 2) the widely used NLSST formulation introduces a correlation between SST gradient magnitudes and SST values. This correlation, likely due to the use of a first guess SST in the NLSST formulation, is not observed in the MCSST data and may affect the study of long-term changes in ocean dynamics.

ARTICLE HISTORY

Received 7 March 2019

Accepted 29 August 2019

1. Introduction

Many studies have demonstrated the pivotal role of ocean fronts in various fields that include marine ecosystems (Belkin, Cornillon, and Sherman 2009), ocean–atmosphere interactions (Sweet et al. 1981; Pyatt et al. 2005; Small et al. 2008), fisheries (Acha et al. 2004), and ocean modelling (Thomas and Ferrari 2008; Ferrari 2011; Levy et al. 2012). Given the impact of ocean dynamics on weather and climate patterns, significant observational efforts have been dedicated to the analysis of spatio-temporal properties of ocean fronts from satellite datasets for the identification of specific spatial patterns and long-term changes (Castel'ao et al. 2006; Belkin and Cornillon 2007; Kahru et al. 2012; Breaker, Mavor, and Broenkow 2005). However, in most of the published literature, the choice of the satellite SST dataset used for the analysis of ocean dynamics is not discussed despite the variety of algorithms used by operational agencies to derive SST

CONTACT M. Bouali  marouan.bouali@usp.br  Instituto Oceanográfico da Universidade de São Paulo (IOUSP), São Paulo 05508–120, Brazil

© 2019 Informa UK Limited, trading as Taylor & Francis Group

from clear-sky Brightness Temperatures (BTs). Furthermore, satellite SST validation metrics like bias and standard deviation with respect to *in situ* measurements do not provide much information on SST gradients at the pixel scale (Wu et al. 2017).

A major challenge in the retrieval of SST from Top-of-Atmosphere BTs besides cloud screening is the absorption and emission of radiation by water vapour and other gases in the atmosphere derived from infrared (IR) measurements. There are currently two major methods used to account for these effects both of which are empirical least square error minimization processes. First, the Multi-Channel Sea Surface Temperature (MCSST) retrieval algorithm (McMillin 1975; Barton 1983; Llewellyn-Jones et al. 1984; McClain, Pichel, and Walton 1985) which, in the dual window case, takes the following form:

$$\text{MCSST} = a_1 + a_2 T_{39} + a_3 (T_{39} - T_4) + a_4 (T_{39} - T_4) (\sec \theta - 1) \quad (1)$$

where T_{39} and T_4 are BTs centred at 3.9 μm and 4 μm , respectively, a_1 to a_4 are coefficients estimated from match-up databases with *in situ* measurements and θ is the satellite zenith angle.

The Nonlinear Sea Surface Temperature (NLSST) (Walton 1988), which was shown to provide similar performances to the MCSST under a wider range of atmospheric conditions takes the following form:

$$\text{NLSST} = a_1 + a_2 T_{11} + a_3 \text{SST}_{\text{ref}} (T_{11} - T_{12}) + a_4 (T_{11} - T_{12}) (\sec \theta - 1) \quad (2)$$

where T_{11} and T_{12} correspond to satellite BTs acquired at 11 μm and 12 μm and SST_{ref} is a 'first guess' or 'reference' SST, typically a Level 4 cloud-free SST field.

When it comes to the analysis of SST values only, these two formulations provide overall similar statistical characteristics (i.e., mean and standard deviation) with respect to each other. Further, the sensitivity of these retrieval schemes to atmospheric water vapour and/or surface temperature can be assessed at synoptic scales using radiative transfer modelling as done in (Merchant et al. 2009). An important question that has not been addressed so far in the literature is how these two retrieval methods differ from each other in terms of geometrical properties of SST fields over large time scales (≥ 1 month), i.e., when analysing SST gradients (vectors with a magnitude and a direction) instead of SST values (points). Therefore, the main goal of this study is to determine whether the MCSST and NLSST lead to similar spatial distributions and temporal variability of SST gradient magnitudes. It should be mentioned that while many other SST retrieval algorithms currently exist (Petrenko et al. 2014), our study focuses only on the two widely used operational schemes NLSST and MCSST.

2. Data and methodology

Our study area is the Southwestern Atlantic Ocean (SAO) which extends from 10°S to 50°S in latitude and from 65°W to 40°W in longitude. In the SAO, the Southward-flowing warm waters of the Brazil Current meet the cold Northward-flowing waters of the Malvinas current, which generates high contrasts in surface heat flux (Sato and

Polito 2014) and strong fronts in surface temperature (Legeckis and Gordon 1982; Garzoli 1993; Bouali, Sato, and Polito 2017). This makes it an interesting location for the comparison of thermal gradients from different SST products.

At the time of writing, operational agencies account for the SST diurnal cycle and distribute two separate SST datasets, i.e., daytime and night-time products generated using the NLSST and MCSST retrieval schemes, respectively. Currently, NASA'S Ocean Biology Processing Group (OBPG) provides both MCSST and NLSST products at night-time from the MODIS instrument onboard the Terra and Aqua platforms. Therefore, the MODIS SST product (Brown and Minnett 1999) constitutes an ideal dataset to investigate the impact of SST retrieval algorithm on derived thermal gradients. In this study, we used the Level 2 Aqua MODIS night-time Short-Wave Infrared (SWIR) 4 μm (MCSST) and Long-Wave Infrared (LWIR) 11 μm (NLSST) datasets acquired from 2005 to 2015 over the SAO region and downloaded from NASA's Ocean Color website <https://oceancolor.gsfc.nasa.gov/>.

The Level 2 data were post-processed to mitigate a major quality issue for the analysis of thermal gradients. Visual inspection of unmasked Level 2 MODIS SST imagery shows that in many cases, sharp thermal fronts are misclassified as clouds and given a quality flag that discards their use for downstream applications. As shown in (Bouali, Sato, and Polito 2017), this can lead to composite maps that significantly underestimate frontal activity in regions known to be highly dynamic. Therefore, the cloud masking strategy used in (Bouali, Sato, and Polito 2017) was applied here. Starting from the Level 2 swath-projection 1 km resolution SST, our processing chain leads to a Level 3 SST field projected into a 0.05° resolution lat/lon grid and denoted hereafter s . For each pixel (i,j) of the grid, we compute the SST gradient magnitude using forward finite differences in the zonal and meridional directions as follows:

$$|\nabla s(i,j)| = \left(\left[\frac{s(i-1,j) - s(i,j)}{d_{i-1,j}^{ij}} \right]^2 + \left[\frac{s(i,j-1) - s(i,j)}{d_{i,j-1}^{ij}} \right]^2 \right)^{1/2} \quad (3)$$

In the previous equation, the notation $d_{i,j-1}^{ij}$ represents the distance in kilometres between pixels (i,j) and $(i,j-1)$ in the lat/lon grid. Composite maps of SST gradient magnitudes are then obtained by averaging all synoptic maps $|\nabla s|$ over the time interval t as:

$$\overline{|\nabla s(i,j)|} = \frac{1}{N_{\text{obs}}^t} \sum_t |\nabla s(i,j)| \quad (4)$$

where N_{obs}^t is the number of clear-sky observations in the time interval t which corresponds to a month, season, year or decade.

3. Results

3.1. Spatial distribution

In this section, we analyse the spatial distribution of SST gradient magnitudes obtained from the NLSST and MCSST formulations. Figure 1 shows seasonal, annual and decadal composite maps of thermal gradients in the SAO. First, we note that despite the high consistency of SST composite maps between NLSST and MCSST (not shown here), the

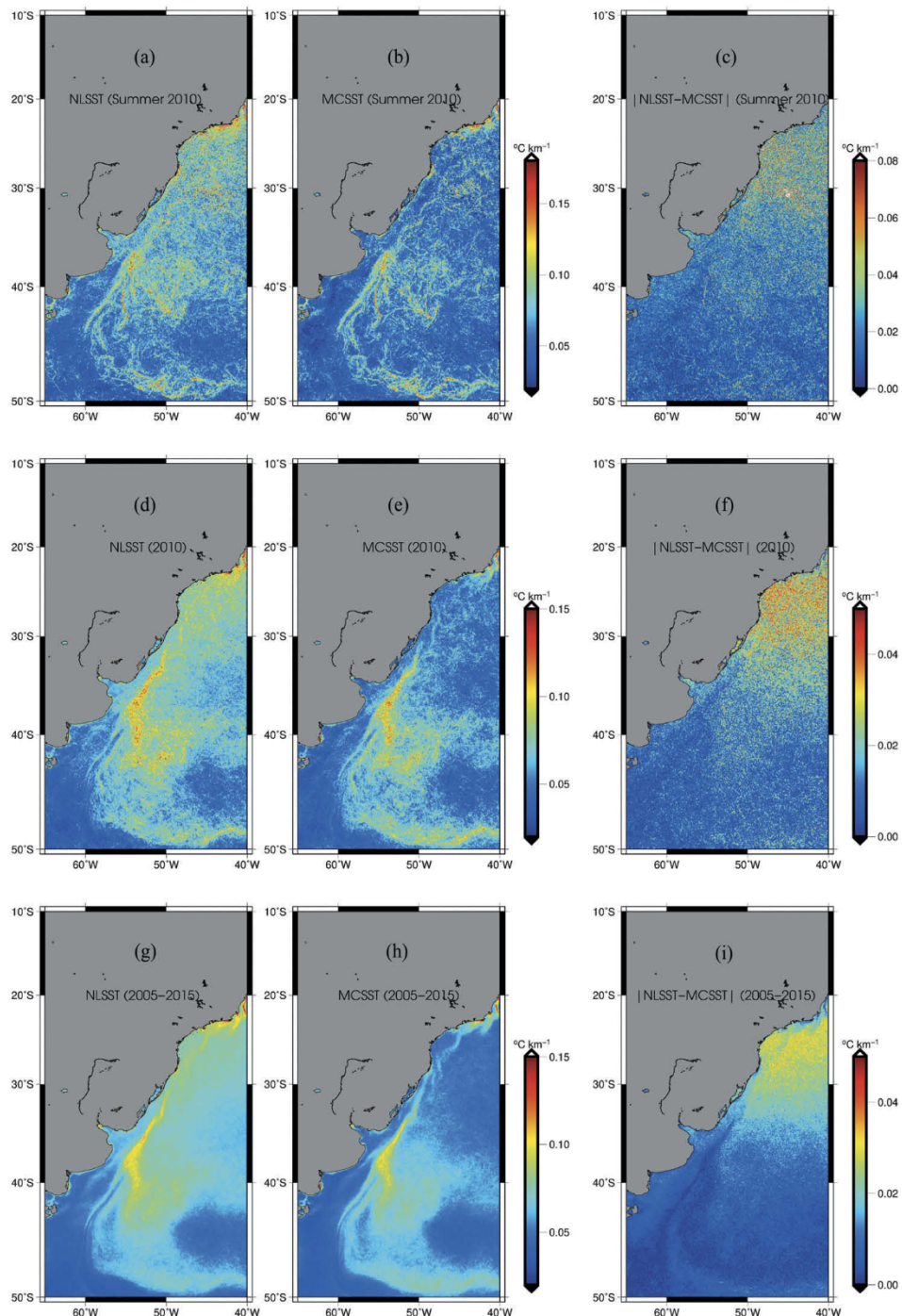


Figure 1. Composite maps of SST gradient magnitudes obtained from the NLSST (a, d, g), MCSST (b, e, h) and their absolute difference (c, f, i) in the SAO region. The composite maps have been derived for the Summer of 2010 (top) the year 2010 (centre) and the entire period from 2005 to 2015.

spatial distribution of SST gradient magnitudes derived from the two retrieval algorithms are different. Seasonal, annual and decadal composite maps from the two retrieval schemes display larger differences over lower latitudes, i.e. warmer surface temperatures. This observed correlation between SST gradient magnitudes and SST values in the case of the NLSST scheme results from the use of the first guess SST term in the retrieval algorithm. In fact, SST_{ref} in Equation 2 acts as a multiplier of the content of the image ($T_{11} - T_{12}$) which is dominated by instrument noise due to the small spectral distance between channels 31 (11 μm) and 32 (12 μm). As can be seen in Figure 2, while individual images from MODIS channels 31 and 32 do not particularly display a major amount of noise, their difference (used for the atmospheric correction) clearly shows the presence of both Gaussian and stripe noise. The difference between MODIS channels 23 (3.9 μm) and 24 (4 μm) also displays a significant amount of stripe noise (figure similar to Figure 2 not shown here) but in the MCSST formulation (Equation 1), it is not multiplied by SST_{ref} . Therefore, the use of SST_{ref} in the NLSST is such that the amount of noise in the derived SST becomes nonlinear, i.e., SST gradients over warm regions are more affected and display higher magnitudes compared to those over colder regions. It should be pointed out that in this study, MCSST and NLSST datasets use different spectral channels. While the MCSST uses spectral bands that are less sensitive to water vapour compared to those used in NLSST, this cannot explain the observed discrepancies in gradients since composite maps of SST gradient magnitude differences (Figure 1 c, 1f and 1i) do not show any correlation with the spatial distribution of water vapour.

The dependency of thermal gradients on SST in the NLSST can be further demonstrated through the analysis of scatter plots for the two retrieval methods, where the two variables of interest are the magnitude of SST gradients, $|\nabla SST|$ (Equation 4) and associated SST values. Figure 3 shows the corresponding scatter plots from monthly, annual and decadal composite maps for the NLSST and MCSST products. We note that regardless of the integration time used for the composite maps, the correlation between the two variables in the NLSST dataset is systematically positive and much higher than that observed in the MCSST which in turn indicates almost no correlation. This observation is further confirmed by comparing the correlation coefficients from monthly

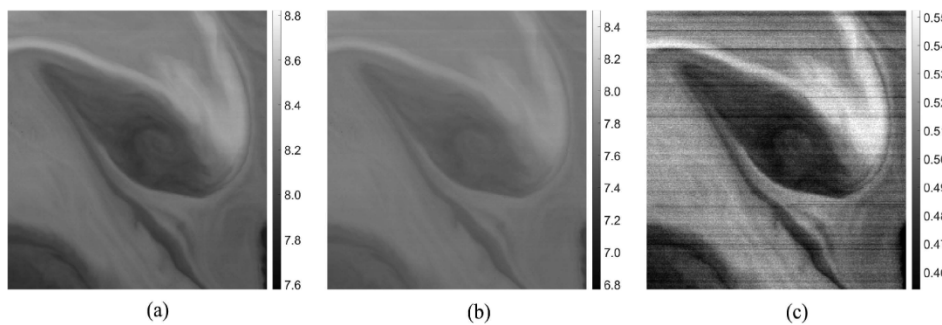


Figure 2. Images of Level 1B radiances from Aqua MODIS channel 31 (a) channel 32 (b) and their difference (c). Note how the difference between channels 31 and 32 contains a significant amount of Gaussian and stripe noise compared to individual bands. The images were captured by Aqua MODIS in the Brazil-Malvinas confluence region on 31 December 2018. Units are in $\text{W m}^{-2} \mu\text{m}^{-1} \text{sr}^{-1}$.

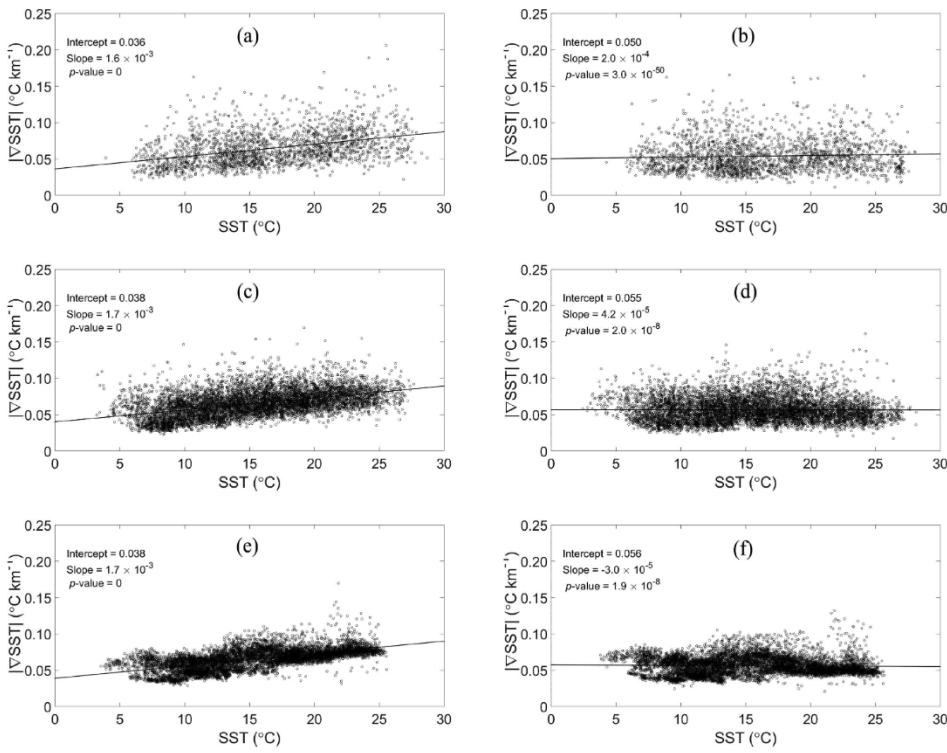


Figure 3. Scatter plots of $|\nabla SST|$ vs SST from the NLSST (left) and MCSST (right) formulations in the SAO region. In the scatter plots each point corresponds to a grid point in the composite maps computed in a time window of summer 2010 (a,b), the year 2010 (c,d) and a decade (2005–2015) (e,f).

Table 1. Correlation coefficient by month between SST gradient magnitudes and SST values from monthly composite maps for NLSST and MCSST.

SST scheme	Correlation coefficient											
	Jan	Feb	Mar	Apr	May	Jun	Jul	Aug	Sep	Oct	Nov	Dec
NLSST	0.2104	0.1831	0.1822	0.1614	0.2001	0.2372	0.2821	0.3461	0.3294	0.3156	0.2620	0.2709
MCSST	-0.0303	-0.0745	-0.0970	-0.0628	-0.0382	0.0176	0.0674	0.0779	0.1073	0.0949	0.0363	0.0432

climatologies derived from the entire period (2005–2015) and reported in Table 1. Consequently, differences in the magnitudes of SST gradients derived from MCSST ($|\nabla MCSST|$) and NLSST ($|\nabla NLSST|$) are clearly dependent on SST values as shown in the scatter plot of Figure 4.

3.2. Temporal variability

In this section, we analyse the temporal variability of thermal gradients observed from NLSST and MCSST datasets to determine whether major discrepancies are observed. Using data from 2005 to 2015, we generated time series of both SST and SST gradient magnitudes where each point represents a monthly average over the entire SAO

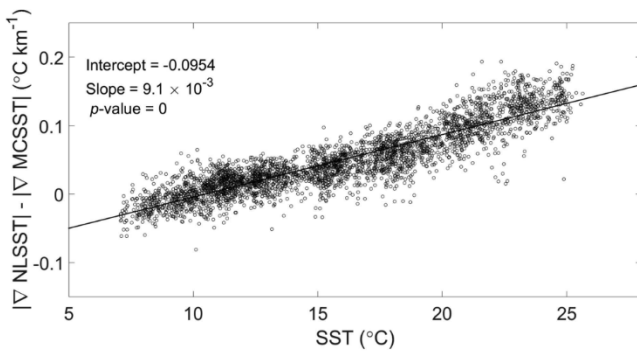


Figure 4. Scatter plots of the error $|\nabla \text{NLSST}| - |\nabla \text{MCSST}|$ vs SST computed using decadal composite maps showing that the difference in the magnitude of SST gradients from the two retrieval schemes is highly correlated to SST.

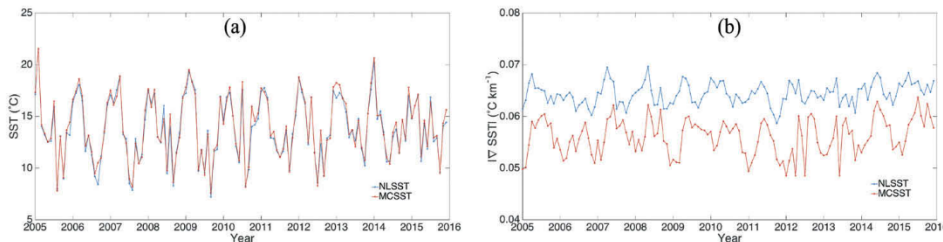


Figure 5. Time series (2005–2015) of SST (a) and SST gradient magnitudes (b) in the Southwestern Atlantic Ocean derived from NLSST and MCSST.

region. This temporal sampling of 1 month was selected to ensure that enough clear-sky pixels are used in the average. In Figure 5, we note significant consistency in the temporal variability of SST values from NLSST and MCSST. However, this consistency does not hold for SST gradient magnitudes which time series derived from the two retrieval schemes indicate a correlation of only 0.45. Further, we also observe a difference in the magnitude of frontal activity derived from the two SST formulations. Over the 2005–2015 time period, SST gradient magnitudes from the NLSST are on average 15% higher than those observed from the MCSST. Using the 11-year time series, we also extracted the annual cycle of SST and SST thermal gradients in the SAO region. As expected, Figure 6 shows almost identical annual cycles of SST derived from NLSST and MCSST with a correlation coefficient of 0.99. This is however not the case for SST gradient magnitudes (Figure 6) where we observe major differences in month-to-month variations as well as in the magnitude of the annual cycle. Although the month of May displays maximum frontal activity for both formulations, minimum SST gradient magnitudes are reached in November for NLSST and in February for MCSST. Also, the annual cycle of frontal activity in the NLSST indicates a monotonic decrease from May to November unlike the MCSST where the magnitude of SST gradients increases again from July to August.

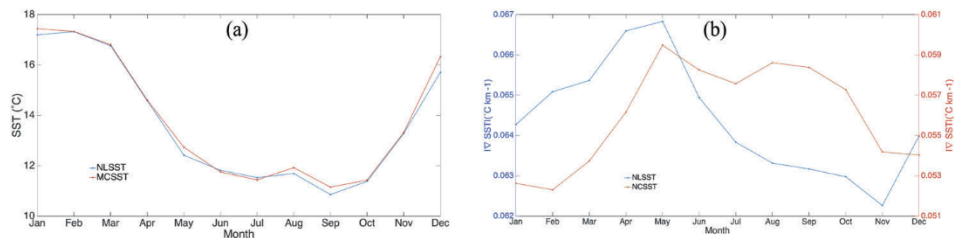


Figure 6. Annual cycle of SST (a) and SST gradient magnitudes (b) in the Southwestern Atlantic Ocean derived from NLSST and MCSST, extracted using data acquired from 2005 to 2015.

4. Conclusions

In this study, we analysed the spatio-temporal characteristics of SST gradient magnitudes in the Southwestern Atlantic Ocean. We used two SST datasets derived from the Aqua MODIS sensor produced with two different SST retrieval schemes, namely the NLSST and the MCSST. Our goal was to determine whether two SST products that are statistically consistent also display similar geometrical properties. Results presented here show that while SST values from the two retrieval methods are consistent, discrepancies are observed when analysing the magnitude of SST gradients. More specifically, the NLSST formulation introduces a clear spatial correlation between SST gradients and SST values that does not appear in the MCSST. This correlation could potentially affect the investigation and interpretation of long-term changes in ocean dynamics over regions with significant temporal trends in SST values. Further, it should be noted that most high resolution Level 4 gap-free SST datasets ingest Level 2 products generated using NLSST which may therefore also display a dependency of SST gradient magnitudes on the SST itself. The observations made here constitute an incentive for future studies on ocean fronts to account for the potential impact of the satellite SST retrieval algorithms on derived SST gradients. A similar study is currently underway which investigates the accuracy of cloud masking at Level 2 and its impact on downstream applications.

Funding

Funding for this research was provided by the Fundação de Amparo à Pesquisa do Estado de São Paulo [2017/04887-0].

References

- Acha, E. M., H. W. Mianzan, R. A. Guerrero, M. Favero, and J. Bava. 2004. "Marine Fronts at the Continental Shelves of Austral South America: Physical and Ecological Processes." *Journal of Marine Systems* 44 (1–2): 83–105. doi:10.1016/j.jmarsys.2003.09.005.
- Barton, I. J. 1983. "Dual Channel Satellite Measurements of Sea Surface Temperature." *Quarterly Journal of the Royal Meteorological Society* 109 (460): 365–378. doi:10.1002/qj.v109:460.
- Belkin, I., and P. Cornillon. 2007. "Fronts in the World Ocean's Large Marine Ecosystems." *International Council for the Exploration of the Sea ICES CM* 2007/D: 21: 33.
- Belkin, I. M., P. C. Cornillon, and K. Sherman. 2009. "Fronts in Large Marine Ecosystems." *Progress in Oceanography* 81 (1–4): 223–236. doi:10.1016/j.pocean.2009.04.015.
- Bouali, M., O. T. Sato, and P. S. Polito. 2017. "Temporal Trends in Sea Surface Temperature Gradients in the South Atlantic Ocean." *Remote Sensing of Environment* 194: 100–114. doi:10.1016/j.rse.2017.03.008.

- Breaker, L. C., T. P. Mavor, and W. W. Broenkow. 2005. "Mapping and Monitoring Large-Scale Ocean Fronts off the California Coast Using Imagery from the GOES-10 Geostationary Satellite." *California Sea Grant College Program*. <http://escholarship.org/uc/item/9mh4f40k>
- Brown, O., and P. Minnett. 1999. "MODIS Infrared Sea Surface Temperature Algorithm." *Algorithm Theoretical Basis Document, Products: MOD28*.
- Castelão, R. M., T. P. Mavor, J. A. Barth, and L. C. Breaker. 2006. "Sea Surface Temperature Fronts in the California Current System from Geostationary Satellite Observations." *Journal of Geophysical Research: Oceans* 111 (C9).
- Ferrari, R. 2011. "A Frontal Challenge for Climate Models." *Science* 332 (6027): 316–317. doi:[10.1126/science.332.6026.173-c](https://doi.org/10.1126/science.332.6026.173-c).
- Garzoli, S. L. 1993. "Geostrophic Velocity and Transport Variability in the Brazil- Malvinas Confluence." *Deep Sea Research Part I: Oceanographic Research Papers* 40 (7): 1379–1403. doi:[10.1016/0967-0637\(93\)90118-M](https://doi.org/10.1016/0967-0637(93)90118-M).
- Kahru, M., E. Di Lorenzo, M. Manzano-Sarabia, and B. Greg Mitchell. 2012. "Spatial and Temporal Statistics of Sea Surface Temperature and Chlorophyll Fronts in the California Current." *Journal of Plankton Research* 34: 749–760. doi:[10.1093/plankt/fbs010](https://doi.org/10.1093/plankt/fbs010).
- Legeckis, R., and A. L. Gordon. 1982. "Satellite Observations of the Brazil and Falkland Currents—1975 1976 and 1978." *Deep Sea Research Part A. Oceanographic Research Papers* 29 (3): 375–401. doi:[10.1016/0198-0149\(82\)90101-7](https://doi.org/10.1016/0198-0149(82)90101-7).
- Levy, M., R. Ferrari, P. J. S. Franks, A. P. Martin, and P. Riviere. 2012. "Bringing Physics to Life at the Submesoscale." *Geophysical Research Letters* 39: 14. doi:[10.1029/2012GL052756](https://doi.org/10.1029/2012GL052756).
- Llewellyn-Jones, D. T., P. J. Minnett, R. W. Saunders, and A. M. Zavody. 1984. "Satellite Multichannel Infrared Measurements of Sea Surface Temperature of the N.E. Atlantic Ocean Using AVHRR/2." *Quarterly Journal of the Royal Meteorological Society* 110 (465): 613–631. doi:[10.1002/\(ISSN\)1477-870X](https://doi.org/10.1002/(ISSN)1477-870X).
- McClain, E. P., W. G. Pichel, and C. C. Walton. 1985. "Comparative Performance of AVHRR-based Multichannel Sea Surface Temperatures." *Journal of Geophysical Research: Oceans* 90 (C6): 11587–11601. doi:[10.1029/JC090iC06p11587](https://doi.org/10.1029/JC090iC06p11587).
- McMillin, L. M. 1975. "Estimation of Sea Surface Temperatures from Two Infrared Window Measurements with Different Absorption." *Journal of Geophysical Research* 80 (36): 5113–5117. doi:[10.1029/JC080i036p05113](https://doi.org/10.1029/JC080i036p05113).
- Merchant, C. J., A. R. Harris, H. Roquet, and P. Le Borgne. 2009. "Retrieval Characteristics of Non-linear Sea Surface Temperature from the Advanced Very High Resolution Radiometer." *Geophysical Research Letters* 36: 17. doi:[10.1029/2009GL039843](https://doi.org/10.1029/2009GL039843).
- Petrenko, B., A. Ignatov, Y. Kihai, J. Stroup, and P. Dash. 2014. "Evaluation and Selection of SST Regression Algorithms for JPSS VIIRS." *Journal of Geophysical Research: Atmospheres* 119 (8): 4580–4599.
- Pyatt, H. E., B. A. Albrecht, C. Fairall, J. E. Hare, N. Bond, P. Minnis, and J. K. Ayers. 2005. "Evolution of Marine Atmospheric Boundary Layer Structure across the Cold Tongue-ITCZ Complex." *Journal of Climate* 18: 737–753. doi:[10.1175/JCLI-3287.1](https://doi.org/10.1175/JCLI-3287.1).
- Sato, O. T., and P. S. Polito. 2014. "Observation of South Atlantic Subtropical Mode Waters with Argo Profiling Float Data." *Journal of Geophysical Research: Oceans* 119 (5): 2860–2881.
- Small, R. J., S. P. deSzeoke, S. P. Xie, L. O'Neill, H. Seo, Q. Song, P. Cornillon, M. Spall, and S. Minobe. 2008. "Air–Sea Interaction over Ocean Fronts and Eddies." *Dynamics of Atmospheres and Oceans* 45 (3–4): 274–319. doi:[10.1016/j.dynatmoce.2008.01.001](https://doi.org/10.1016/j.dynatmoce.2008.01.001).
- Sweet, W., R. Fett, J. Kerling, and P. La Violette. 1981. "Air–Sea Interaction Effects in the Lower Troposphere across the North Wall of the Gulf Stream." *Monthly Weather Review* 109 (5): 1042–1052. doi:[10.1175/1520-0493\(1981\)109<1042:ASIEIT>2.0.CO;2](https://doi.org/10.1175/1520-0493(1981)109<1042:ASIEIT>2.0.CO;2).
- Thomas, L., and R. Ferrari. 2008. "Friction, Frontogenesis, and the Stratification of the Surface Mixed Layer." *Journal of Physical Oceanography* 38 (11): 2501–2518. doi:[10.1175/2008JPO3797.1](https://doi.org/10.1175/2008JPO3797.1).
- Walton, C. C. 1988. "Nonlinear Multichannel Algorithms for Estimating Sea Surface Temperature with AVHRR Satellite Data." *Journal of Applied Meteorology* 27: 115–124. doi:[10.1175/1520-0450\(1988\)027<0115:NMAFES>2.0.CO;2](https://doi.org/10.1175/1520-0450(1988)027<0115:NMAFES>2.0.CO;2).
- Wu, F., P. Cornillon, B. Boussidi, and L. Guan. 2017. "Determining the Pixel-to-Pixel Uncertainty in Satellite-Derived SST Fields." *Remote Sensing* 9 (9). doi:[10.3390/rs9090877](https://doi.org/10.3390/rs9090877).